IJE TRANSACTIONS B: Applications Vol. 31, No. 2, (February 2018) 339-345

International Journal of Engineering

Journal Homepage: www.ije.ir

Design, Optimization and FEM Analysis of a Surface-Mounted Permanent-magnet Brushless DC Motor

H. Moradi Cheshmeh Beigi*

Electrical Engineering Department, Faculty of Engineering, Razi University, Kermanshah, Iran

PAPER INFO

Paper history:
Received 28 April 2017
Received in revised form 15 September 2017
Accepted 02 October 2017

Keywords:
Surface-mounted PM Brushless DC motor
Finite Element Analysis
Analytical Model

ABSTRACT

In this paper a fast analytical algorithm for design a surface-mounted PM Brushless DC motor (SMPM-BLDC) for variable-speed application based on electromagnetic field analysis and RSM optimization algorithm is discussed. To achieve the desired performance, the physical dimensions of the proposed SMPM-BLDC motor subject to minimal ripple torque utilizing RSM optimization algorithm were optimized. Finally, to evaluate the motor performance and confirm the accuracy of the proposed design procedure 2-D Finite Element (FE) analysis were employed. The obtained numerical analysis results explain the accuracy and effectiveness of the proposed machine design methodology.

***doi**: 10.5829/ije.2018.31.02b.19*

NOMENCLATURE

P_{out}, I_{phase}	Rated power output, Rated phase current	h_{ry}, h_{ts}	The height of the rotor yoke, The stator tooth width,
E_{phase}	Rated phase voltage	B_{st}	Maximum stator teeth flux density,
ω_{rated}	Rated speed	h_{st}, D_i	The stator slot height, The shaft diameter,
L, D_{ro}	Active motor length, Rotor outer diameter	K_s	The slot packing factor,
h_{sy}, T	The height of the stator yoke, Motor developed torque	D_y	The outer stator diameter,
N_{coil}	Number of coils conducting simultaneously	A_{sl}, l_f	The stator slot area, The lamination factor,
N_m, N_ζ	Number of pole, Number of slot/pole/phase	Φ_{tm}	The flux into this stator tooth,
k_j	The stacking factor of the stator iron laminations	B_{st}	The stator tooth flux density,
K_w, B_g	Winding factor, Specific magnetic loading	f_f, A_s	The slot fill factor, The slot area,
I_s, Q_s	Specific slot loading, The number of stator slots,	ρ_c	The resistivity of the wire at its operating temperature,
B_{sy}	The maximum flux density in the stator yoke,	l_c	The length of one turn of the winding coils,
ω_s, t_t	Slot width, Tooth width	l_{ext}	The coil-end extension length and is a value generally between 10 and 30 mm,
B_m	The flux density in the Air-Gap above the magnets,	τ_y, β	The coil pitch, The short pitch ratio,
l_g	The equivalent Air-Gap length	I_a, ρ	The RMS phase current, The resistive of copper,
h_m, D_{rc}	The magnet thickness, The rotor core diameter	ω_{elec}	The electrical angular velocity,
r	Stands for the radius at which the flux density is calculated	A_s, A_{cond}	The slot area, The conductor area,
Φ_{sy}	The maximum flux in the stator yoke,	N_s	The number of slot,
B_{sy}, α	The stator yoke flux density, The half pole angle,	N_w, L_{st}	number of turns per phase, axial length of the motor,
h_{sy}, B_{ry}	height of the stator yoke, Maximum rotor yoke flux density	R_{r0}, B_g	The air gap radius at the magnet surface, The air gap flux density,
$l_g$and A_g	The air gap length and cross-sectional area respectively,	$l_m$and Am	The magnet length and cross-sectional area respectively,

*Corresponding Author's Email:ha.moradi@razi.ac.ir(H. Moradi CheshmehBeigi)

Please cite this article as: H. Moradi CheshmehBeigi, Optimization and FEM Analysis of a Surface-mounted Permanent-magnet Brushless DC Motor,International Journal of Engineering (IJE),IJE TRANSACTIONS B: Applications Vol. 31, No. 2, (February 2018) 339-345

INTRODUCTION

Variable-speed applications such as hybrid electric cars, aircraft and buses required fault-tolerance, high efficiency, low inertia, high torque/volume and maintenance free machine. The permanent-magnet brushless DC (PM BLDC) machine are popular for variable-speed applications due to their aspects. The PMBLDC machine inherently offers the advantages of high efficiency, high power density and maintenance-free operation. However, because of the uncontrollable PM electromagnetic flux, it suffers from a short constant-power operating range. To overcome this problem, the field-oriented flux-weakening control and the advanced conduction angle control were developed [1]. By improving the technology of high energy density PM materials not only reduces the size and the amount of losses, but also improves the efficiency of PMBLDC machines [2, 3].

A review on PMBLDC motors and control strategies with detailed aspects has been reported in literature [4]. Design, optimization, numerical analysis and torque capability study for BLDC motor is also discussed in literature [5, 6]. Yang et al. [7] have investigated design of a high-efficiency minimum-torque-ripple 12-V/1-kW 3-phase BLDC motor drive system for diesel engine has been studied. Also, design optimization of asymmetric air-gap structure for small 3-phase permanent magnet SPM BLDC motor were developed [8]. Jung et al [9] have studied on the effect of the magnetization direction on the iron loss characteristics in brushless DC motors. Qu et al. [10] have proposed an improved torque density and efficiency dual rotor, radial-flux BLDC motor. Comparisons of radial and axial field BLDC machines have been discussed by Sitapatiand Krishnan [11]. Another PM motor has been presented in literature [12-14]. Cheshmehbeigi and Khanmohamadian [12] have investigated on design and simulation of a moving-magnet-type linear synchronous motor for electromagnetic launch system. Multi-objective optimal design of a five-phase fault-tolerant axial flux PM motor has been discussed by Saavedra Ordóñez [13]. Vaez-Zadeh and Zamanian [14] have presented permanent magnet DC motor sliding mode control system.

The present paper approaches the design process based on fast analytic algorithm and FEM analysis for a three phase, salient pole PMBLDC for Variable-Speed application. In order to achieve the desired performance and aspects, the physical dimension of the PMBLDC motor should be minimized via utilization of RSM optimization algorithm. 2-D Finite element (FE) analysis was carried out to evaluate the motor performance and to confirm the accuracy of the proposed design procedure.

PROPOSED SMPM-BLDC MOTOR STRUCTURE and DESCRIPTION OF THE DESIGN ALGORITHM

The proposed BLDC motor in this paper is a surface-mounted PM synchronous motors which the PM are mounted on the outer surface of the rotor. Mounting the PM to the surface of the rotor is the cheapest and simplest method for construction of this group of electrical machines. An essential advantage of this specific design is yielding a rotor with small diameter and small inertia, which is suitable for fast dynamic application.

❖ Design Process

Explaining the limitations and requirements of operation, is the first step of design process. The design specs, some constraints and target values are summarized in Table 1.

As shown in Figure 1, structure of the addressed machine in this paper is the 9/6 poles, surface-mounted PM type BLDC motor. The merit of this configuration is that all of the produced magnetic flux by the magnets links the stator and therefore takes part in energy conversion.

TABLE 1. The Constraints and Application Goals of the Design

Design Specifications	Constraints and Targets	
Rated Power	1500	W
Rated Speed	3500	rpm
Maximum Speed	4500	rpm
Phase Voltage	48	V
Outer Dimensions of the Motor	Dimension of the Available Space	
Total Length	100	mm
Outer Stator Diameter	150	mm

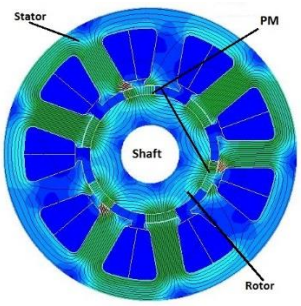

Figure 1. 9/6 poles, surface-mounted magnet BLDC Motor

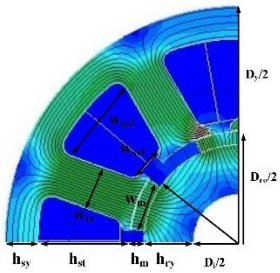

Figure 2. main dimension for proposed SMPM-BLDC motor

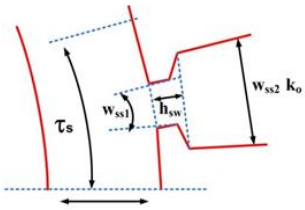

Figure 3. Tooth and slot parameters

The main dimension for proposed SMPM-BLDC motor is shown in Figure 2. The output equation for PM BLDC motor is derived as follows [1-3]:

$$P_{out} = T\omega_{rated} = \eta N_{coil} E_{phase} I_{phase} \quad (1)$$

$$T = \frac{P_{out}}{\omega_{rated}} = \frac{\eta N_{coil} E_{phase} I_{phase}}{\omega_{rated}} = \frac{\eta N_{coil}\left(\frac{N_m N_\zeta K_w B_g L D_{ro} n_s \omega_{rated}}{2}\right) I_{phase}}{\omega_{rated}} = \frac{L D_{ro} \eta N_{coil} N_m N_\zeta K_w B_g I_s}{2} \quad (2)$$

$$LD_{ro} = \frac{2T}{\eta N_{coil} N_m N_\zeta K_w B_g I_s} \quad (3)$$

$\frac{D_{ro}{}^2}{L}$ is an important parameter in design process which by choosing a proper value for $\frac{D_{ro}{}^2}{L}$, D_{ro} and L can be calculated, and:

$$t_t = (1 - \omega_s).\tau_s \ , 0.5\tau_s < \omega_s < 0.6\tau_s \quad (4)$$

In this analysis, the approximation is the equality of slot and tooth width values:

$$\omega_s \approx t_t \quad (5)$$

Figure 3 shows the tooth and slot parameters of under study motor. One of the fundamental factors that should be considered in design process is the number of poles. Utilizing a higher pole number decreases the stator back thickness and the end winding length. It should be noted that choosing the high pole number, increase the magnet flux leakage. The maximum air-gap flux density is given by Equation (6):

$$B_m(r) = \frac{h_m B_r}{r.\left[\ln\left(\frac{D_{rc}+2.h_m}{D_{rc}}\right) + \mu_r.\ln\left(\frac{D_{rc}+2.h_m+2.l_g}{D_{rc}+2.h_m}\right)\right]} \quad (6)$$

the maximum flux in the stator can be expressed as follows:

$$\Phi_{sy} = 0.5\Phi_{mp} = B_{sy} h_{sy} k_j L \quad (7)$$

the height of the stator yoke can be calculated as:

$$h_{sy} = \frac{\alpha B_m.(D - 2l_g)}{p.k_j.B_{sy}} \quad (8)$$

the height of the rotor yoke is given by Equation (9):

$$h_{ry} = \frac{\alpha B_m.(D - 2l_g)}{p.k_j.B_{ry}} \quad (9)$$

the stator tooth height can be expressed as Equation (10):

$$h_{ts} = \frac{B_m.\pi(D - 2.l_g)}{Q_s.k_j.B_{st}} \quad (10)$$

the stator slot area can be calculated by Equation (11):

$$A_{s1} = (h_{st} - h_{sw})\frac{w_{ss1} + w_{ss2}}{2} \quad (11)$$

l_f is the lamination factor and is usually between 0.95 and 1. If the rotor of SMPM-BLDC machines is not laminated, then $l_f = 1$. When the center line of a rotor pole is aligned with a stator tooth, the flux into this stator tooth reaches its maximum (denoted by Φ_{tm}). The stator tooth width calculated as follows:

$$w_{ts} = \frac{\Phi_m}{B_{st} L l_f} \quad (12)$$

the slot area can be calculated as follows:

$A_s = \frac{6N_c A_{cu}}{N_s f_f}$, (f_f, Typically 0.6 to 0.7) (13)

the copper wire is stated as follows:

$A_{wire} = \frac{I}{J_s}$, (J_s , Typically 3 to 7 A/mm^2) (14)

the stator slot pitch is stated as follows:

$$\tau_s = \pi.\frac{\left(D_{ro}/2\right) - l_g}{Q_s} \quad (15)$$

the ampere loading summed as stated as follows:

$$A = \frac{6N_{coils} I_{rms}}{\pi D_i} \quad (16)$$

the current density is stated as follows:

$$J_s = \frac{6N_{coils} I_{rms}}{K_{sf} N_s A_{slot}} \quad (17)$$

the number of coils per phase is given below:

$$N_{coils} = 2qpN \quad (18)$$

the conductor diameter is stated as follows:

$$d_c = \sqrt{\frac{2N_s K_{sf} A_{slot}}{3\pi N_{coils}}} \quad (19)$$

The magnet characteristics are assumed as follows

Flux density	B_r	1.1 T

Demagnetization flux density	B_D	-0.2 T
Relative magnet permeability	μ_r	1.05
A reasonable design has the following flux densities		
Air-Gap flux density	B_g	0.85 - 0.95 T
Maximum flux density in the rotor yoke	B_{ry}	1.4 T
Maximum flux density in the stator yoke	B_{sy}	1.4 T
Maximum flux density in the stator teeth	B_{st}	1.8 T(near to saturation)

• To prevent faced along with high temperatures and insulation, the maximum current density J_s should be lower than 7 $^{A}/_{mm2}$. This value is relevant for a motor without forced cooling. Depending on the way the motor is cooled, higher current densities could be achievable. The copper loss P_{cop} is given by $3I^2R_{cu}$, where R_{cu} is the stator armature resistance per phase.

$$R_{dc} = \rho_c \frac{l_c N_c}{A_{cu}} \tag{20}$$

$$l_c = 2(L + l_{end}) \tag{21}$$

$$l_{end} = 2l_{ext} + \tau_y \tag{22}$$

$$\tau_y = \frac{\pi(D + 2(H_{s0} + H_{s1}) + \mathrm{H}_{s2})}{P}\beta \tag{23}$$

the amplitude of the phase back-EMF is given by expression:

$$e_{ph} = N_w D_s I_a B_g \frac{\omega_{elec}}{p} \tag{24}$$

and the electromagnetic torque is obtained as stated as follows:

$$T = 2N_w D_s I_a B_g \tag{25}$$

while the copper loss is given below:

$$P_{cu} = 2I_a^2 \rho \frac{2N_w I_a}{A_{cond}} = 24N_w^2 I_a^2 \rho \frac{I_a}{A_s K_s N_s} \tag{26}$$

where the cross-sectional area of the conductors is stated as follows:

$$A_{cond} = \frac{\frac{A_s}{2} K_s}{\frac{3N_w}{N_s}} \tag{27}$$

TWO DIMENSIONAL FEM ANALYSES

Calculation of magnetic field characteristics for the machine parameters done accurately with FE techniques by applying precise machine geometry and materials properties. FEM has the ability to take into account the effects of magnetic field saturation based on machine performance. In this paper magnetic field analysis based on variational energy minimization technique (known as T-Ω formulation) was performed by employing Magnet CAD package to determine the magnetic vector potential [15, 16].

$$\nabla.\mathrm{T} - \nabla.(\nabla\Omega) = 0 \tag{28}$$

$$\begin{cases} \nabla^2\mathrm{T} - \mu\sigma\left(\frac{\partial \mathrm{T}}{\partial \mathrm{t}}\right) = -\mu\sigma\nabla\left(\frac{\partial\Omega}{\partial \mathrm{t}}\right) \\ \nabla^2\Omega = 0 \end{cases} \tag{29}$$

T Electric vector potential, Ω Magnetic scalar potential,

T *and* $\Omega$are defined by $\mathrm{j} = \nabla \times \mathrm{T}$ and $\mathrm{H} = \mathrm{T} - \nabla\Omega$

The detailed derivation are discussed in literature [15]. In order to simplify the FE modeling problem a few assumptions have been made. To solve the problem with 2-D FEM analysis, the computed quantities were assumed to remain constant when considering different sections of the machine; also the materials of which the machine is made are considered to be isotropic. In this research for precise solution of Maxwell's equations and calculate the field analysis finite element technique is employed by utilizing a MagNet CAD package (Infolytica Corporation Ltd., 2007).

RESPONSE SURFACE METHOD (RSM) OPTIMIZATION ALGORITHM

RSM is a non-deterministic method for constructing global estimates to system behavior based on results calculated at different points in the design space. This method's advantage is in its reliable approximation for real experimental systems, which requires heavy computations, when sensitivity is not available and the batch run is impossible. But it is limited with errors caused by the nature of approximation [17, 18]. The most important sources of noise in designed BLDC motor are the ripple and cogging torque, which interacts between PMs and the stator teeth and cause vibration and speed perturbation. These undesirable effects cannot be reduced, unless an optimal PM shape is obtained through the optimization process.

In this paper, in order to reach to an acceptable result, RSM was used for the multi-quadric radial basis. The optimization technique has wide spread application in global interpolation, furthermore has the fitting ability when a limited number of experimental data is available. In first step, let's introduce the optimization algorithm. Response surface in a designed space can be modeled with following equations:

$$M(x) = \sum_{i=1}^{N} k_i l(x - x_i) \tag{30}$$

$$l(x) = \sqrt{x^2 + c^2} \tag{31}$$

Where x is the design parameter vector, k_i is the weight factor corresponding to the i th experimental data, $l(x)$ is the multi-quadric radial basis function, and c is the shape parameter of the design. To determine k_i the weight factor, for a set of experimental data, one just have to solve the following equation:

$$X = \{((x_i, j(x_i)), i = 1, 2, ..., N\} \text{ Set of Given practical data} \quad (32)$$

$$j(x_k) = \sum_{i=1}^{N} k_i l(x_k - x_i), k = 1, 2, ..., N \text{ Determining weight factor} \quad (33)$$

As it is obvious, the shape parameter plays the most important role in fitting performance of RSM and its value is required to be chosen very carefully to have near-real approximations. Rippa [17] has utilized $c = 0.815 \sum_{i=1}^{N} \frac{d_i}{N}$, where d_i is the distance between the i th experimental data and its nearest neighbor. It is also defined $c = 1.25 D/\sqrt{N}$, where D is the diameter of the minimal circle enclosing all experimental data, and N is the number of achieved practical data [17]. Choices of these values are dependent to the nature of design procedure. The quality of the computed response surface (i.e., interpolation error) can be evaluated after choosing a value for shape parameter, by 'sequential leave one out' method, which is outlined briefly. After removing a solitary data $(x_k, j(x_k))$ from the original set X , interpolation error can be defined as follows:

$$R(c) = \sum_{k=1}^{N} \sqrt{R^2}_k / N \quad (34)$$

$$R_k(c) = j(x_k) - M^{(k)}(x_k), k = 1, 2, ..., N \quad (35)$$

Where newly constructed set of experimental data is $X^{(k)}$ and the corresponding error is $M^{(k)}$.

But in the situation, where there are a fixed number of experimental data available, optimization occurs just through a good choice of shape parameter, because as mentioned it has the most vital effect on constructing the global response surfaces in algorithm introduced. Next step is adapting RSM with the designed BLDCM. After constructing the response surfaces, to obtain a minimal point, which is deeply dependent on the quantity of available experimental data, several different methods, which satisfy this aim can be used, but the most applicable one "(1+1) evolution strategy" was employed to produce the final results. While in stochastic observation, it was proved that increasing number of experimental data results in decreasing the corresponding interpolation error, but also it should be considered that to achieve a large number of points when using the finite-element method, which lessens the error and produces result closer to real value, more computation time is required. For the designed BLDC motor, in regions where a large interpolation error is expected, in order to alleviate required computing time, additional experimental data was adaptively employed. Previously, Pan Seok Shin et al. [18] have conducted observation over shape optimization of large-scale BLDC motor. Interpolation error can be defined over the kth experimental data as the following equation:

$$E_g(x_k) = \left\| \frac{\nabla F_{abj}(x_k)}{\|\nabla F_{abj}(x_k)\|} - \frac{\nabla M(x_k)}{\|\nabla M(x_k)\|} \right\| \quad (36)$$

$F_{abj}(x)$ is the objective function, $M(x)$ is the response surface. Optimized response surfaces constructed both with original and additional data exhibit decreased corresponding error; thus, closer to real values. By repeating this process, adding adapted data in regions where a large error is expected, better response surfaces would be obtained.

NUMERICAL ANALYSIS RESULTS

Complete model geometry, meshing, material properties and boundary conditions are pre-processing FEM analysis requirement. Figure 6 shows the no-load magnetic flux density for different rotor position (θ=0 °and 60° rotor position). The value of flux density in different parts of the permanent magnet motor design is one of the important parameters. This parameter in core losses and the core saturation is very impressive.

In proposed structure an important design parameter is the air-gap flux density which has significant effect on the machine features. Therefore, this parameter must be chosen carefully. Figure 7 shows the air-gap flux density at no-load and the flux-current characteristics at different rotor positions.

Figure 8 shows distributed flux density at no load for different rotor position. The back EMF, cogging torque and the PM flux can be determined from the no-load field distribution.

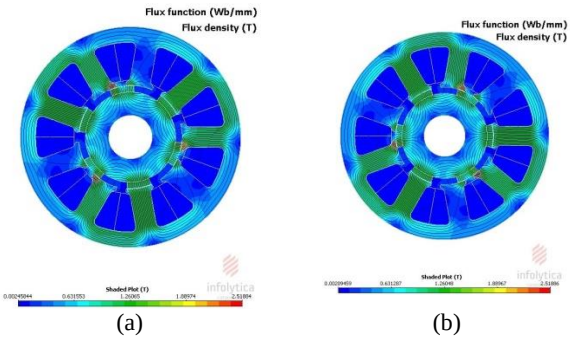

(a) (b)

Figure 6. Magnetic flux density for different rotor position at no-load (θ=0 °and 60° rotor position).

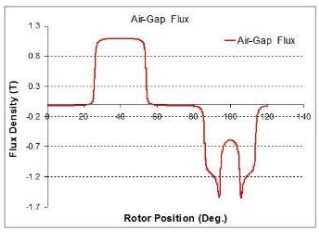

a- Air-Gap flux density at no-load

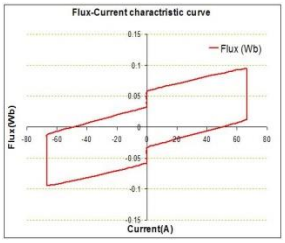

b- The flux-current character

Figure 7. The Air-Gap flux density at No-Load and the Flux-current characteristic

Figure 8 shown the induced line and phase Back-EMF waveforms in stator winding in rotor speed ω_r. Cogging torque and torque profile of designed motor under 100% and 75% rated currents are presented in Figure 9. To achieve the required efficiency, the physical dimensions of the proposed structure is optimized in order to reduce torque ripple. For next step of design procedure, RSM optimization algorithm was employed subject to minimal ripple torque.

Figure 10 shown the results of optimized value for w_{ts}. Figure 10-a shown the influence of $w_{ts} = 22°, 25° \; and \; 28°$ on the torque profile. The rotor pole Span has crucially effect on the T_{ave} and T_{rip}, as it can be seen in Figure 10-b. The T_{rip} decreases with increasing w_{ts}. The T_{ave} can be increased by growing w_{ts}. Table 2 summarized specifications of the designed machine.

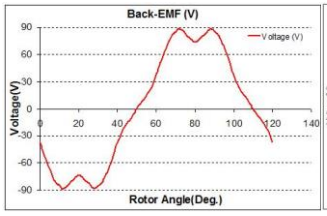

a- Phase Back-EMF waveform

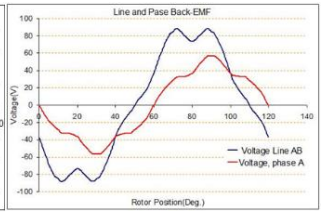

b- Line and phase Back-EMF waveform

Figure 8. Line and phase Back-EMF waveforms

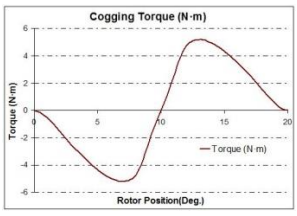

a- Cogging torque profile

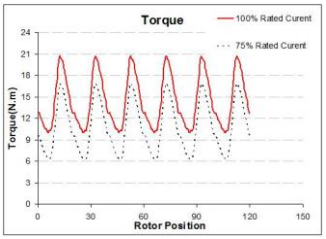

b- Torque-Rotor Position profile

Figure 9. Cogging torque and Torque profile of designed motor

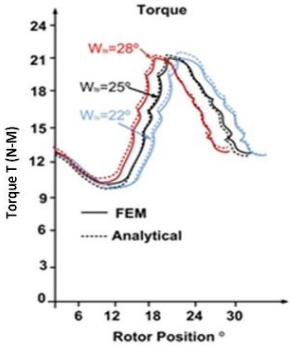

a- Changing Rotor Pole width - Cogging Torque

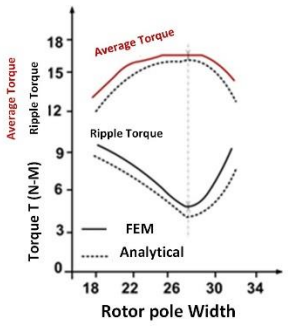

b- Changing Rotor Pole width - T_{Ave} and T_{Rip}

Figure 10. Influence of changing rotor pole width a- Torque profile and b- Average Torque and Ripple Torque

TABLE 2. Specifications of the designed machine

Specifications	Value	Dim
Supply voltage	48	V
Rated current	34	A
Rated speed	3500	rpm
Motor outer diameter	142	mm
Air gap thickness	0.3	mm
Stack length	90	mm
Rotor type	Surface mounted with radial magnets	
Number of poles	6	
Number of phases	3	
Number of slots	9	
Magnet material	Neodymium Iron Boron	
Core thickness	15	mm
Rotor Inner diameter	28	mm
Rotor Outer diameter	66	mm
Magnet angle	28	Deg.
Magnet thickness	4	mm
Back iron depth	10	mm
Stator Inner diameter	66.6	mm
Stator Outer diameter	142	mm

CONCLUSION

The designed PMBLDC motor in this paper could be used as a starter in the electric vehicle application. To evaluate the motor performance and confirm the accuracy of the proposed design procedure 2-D finite element (FE) analysis were employed. The effectiveness of utilized analytical technique were confirmed by validation of obtained results.

REFERENCES

1. Hendershot, J.R. and Miller, T.J.E., "Design of brushless permanent-magnet machines, Motor Design Books, (2010).
2. Gieras, J.F., "Permanent magnet motor technology: Design and applications, CRC press, (2002).
3. Hanselman, D.C., "Brushless permanent magnet motor design, The Writers' Collective, (2003).
4. Pillay, P. and Freere, P., "Literature survey of permanent magnet ac motors and drives", in Industry Applications Society Annual Meeting, 1989., Conference Record of the 1989 IEEE, (1989), 74-84.
5. Binns, K. and Shimmin, D., "The relationship between performance characteristics and size of permanent magnet motors", Proc. Elect. Drives Conf., (1995), 423–427.
6. Huang, S., Luo, J., Leonardi, F. and Lipo, T.A., "A general approach to sizing and power density equations for comparison of electrical machines", ***IEEE Transactions on Industry Applications***, Vol. 34, No. 1, (1998), 92-97.
7. Yang, F., Jiang, C., Taylor, A., Bai, H., Kotrba, A., Yetkin, A. and Gundogan, A., "Design of a high-efficiency minimum-torque-ripple 12-v/1-kw three-phase bldc motor drive system for diesel engine emission reductions", ***IEEE Transactions on Vehicular Technology***, Vol. 63, No. 7, (2014), 3107-3115.
8. Kam, S.-H. and Jung, T.-U., "A design optimization of asymmetric air-gap structure for small 3-phase permanent magnet spm bldc motor", ***Journal of Magnetics***, Vol. 20, No. 1, (2015), 91-96.
9. Jung, J.-W. and Kim, T.-H., "A study on the effect of the magnetization direction on the iron loss characteristics in brushless dc motors", ***Journal of Magnetics***, Vol. 15, No. 1, (2010), 40-44.
10. Qu, R. and Lipo, T.A., "Dual-rotor, radial-flux, toroidally wound, permanent-magnet machines", ***IEEE Transactions on Industry Applications***, Vol. 39, No. 6, (2003), 1665-1673.
11. Sitapati, K. and Krishnan, R., "Performance comparisons of radial and axial field, permanent-magnet, brushless machines", ***IEEE Transactions on Industry Applications***, Vol. 37, No. 5, (2001), 1219-1226.
12. Cheshmehbeigi, H.M. and Khanmohamadian, A., "Design and simulation of a moving-magnet-type linear synchronous motor for electromagnetic launch system", ***International Journal of Engineering-Transactions C: Aspects***, Vol. 30, No. 3, (2017), 351.
13. Saavedra Ordóñez, H., Riba Ruiz, J.-R. and Romeral Martínez, J.L., "Multi-objective optimal design of a five-phase fault-tolerant axial flux pm motor", ***Advances in Electrical and Computer Engineering***, Vol. 15, No. 1, (2015), 69-76.
14. Vaez-Zadeh, S. and Zamanian, M., Permanent magnet dc motor sliding mode control system, in Magnetic and superconducting materials: Volume 2. 2000, World Scientific.1081-1088.
15. Ren, Z., "T-/spl omega/formulation for eddy-current problems in multiply connected regions", ***IEEE Transactions on Magnetics***, Vol. 38, No. 2, (2002), 557-560.
16. Magnet, C., "Package: User manual", ***Infolytica Corporation Ltd., Montreal, Canada***, Vol., No. 0.005, (2006), 0.01.
17. Rippa, S., "An algorithm for selecting a good value for the parameter c in radial basis function interpolation", ***Advances in Computational Mathematics***, Vol. 11, No. 2-3, (1999), 193-210.
18. Shin, P.S., Kim, H.-D., Chung, G.-B., Yoon, H.S., Park, G.-S. and Koh, C.S., "Shape optimization of a large-scale bldc motor using an adaptive rsm utilizing design sensitivity analysis", ***IEEE Transactions on Magnetics***, Vol. 43, No. 4, (2007), 1653-1656.

Design, Optimization and FEM Analysis of a Surface-Mounted Permanent-magnet Brushless DC Motor

H. Moradi CheshmehBeigi

Electrical Engineering Department, Faculty of Engineering, Razi University, Kermanshah, Iran

P A P E R I N F O

Paper history:
Received 28April 2017
Received in revised form 15September 2017
Accepted 02October 2017

Keywords:
Surface-mounted PM Brushless DC motor
Finite Element Analysis
Analytical Model

چکیده

در این مقاله با بهره‌گیری از یک روش تحلیلی، طراحی و بهینه سازی یک موتور جریان مستقیم بدون جارویک برای کاربردهای سرعت متغییر ارایه شده است. برای دستیابی به مشخصات مورد نیاز، ابعاد فیزیکی ماشین با تابع هدف کاهش ریپل گشتاور با استفاده از روش RSM بهینه‌سازی شده است. برای نشان دادن کارایی ساختار مورد مطالعه، ساختار BLDC پیشنهادی با یک ساختار مشابه ولی بدون آهنربای دائم مقایسه شده‌است. نهایتا برای ارزیابی کارایی ساختار پیشنهادی و دقت پروسه طراحی روش آنالیز عددی المان محدود دو بعدی استفاده شده است. نتایج بدست آمده از آنالیز عددی دقت روش طراحی ساختار پیشنهادی را تصدیق می نماید.

***doi**: 10.5829/ije.2018.31.02b.19*